Reliability Sensitivity Analysis and Design Optimization of Composite Structures Based on Response Surface Methodology

Report for Grant: NAG 1-02099

Period of Performance: May 2002 - May 2003

Principal Investigator:

Masoud Rais-Rohani, PhD, PE
Professor
Department of Aerospace Engineering
Mississippi State University
Mississippi State, MS 39762
Phone: (662) 325-7294
Fax: (662) 325-7730
E-mail: masoud@ae.msstate.edu

Submitted to:

Mechanics and Durability Branch
Mail Stop 190
NASA Langley Research Center
Hampton, VA 23681

Abstract

This report discusses the development and application of two alternative strategies in the form of global and sequential local response surface (RS) techniques for the solution of reliability-based optimization (RBO) problems. The problem of a thin-walled composite circular cylinder under axial buckling instability is used as a demonstrative example. In this case, the global technique uses a single second-order RS model to estimate the axial buckling load over the entire feasible design space (FDS) whereas the local technique uses multiple first-order RS models with each applied to a small subregion of FDS. Alternative methods for the calculation of unknown coefficients in each RS model are explored prior to the solution of the optimization problem. The example RBO problem is formulated as a function of 23 uncorrelated random variables that include material properties, thickness and orientation angle of each ply, cylinder diameter and length, as well as the applied load. The mean values of the 8 ply thicknesses are treated as independent design variables. While the coefficients of variation of all random variables are held fixed, the standard deviations of ply thicknesses can vary during the optimization process as a result of changes in the design variables. The structural reliability analysis is based on the first-order reliability method with reliability index treated as the design constraint. In addition to the probabilistic sensitivity analysis of reliability index, the results of the RBO problem are presented for different combinations of cylinder length and diameter and laminate ply patterns. The two strategies are found to produce similar results in terms of accuracy with the sequential local RS technique having a considerably better computational efficiency.

1. Introduction

The desire to increase structural efficiency while maximizing reliability and robustness has fueled the rapid growth of non-deterministic approaches for more than a decade, and has led to the development and application of many techniques under the general category of reliability-based optimization (RBO). Numerous techniques have been developed to assess the structural reliability of a component or a system, which can be broadly categorized into two groups: (1) random sampling methods, and (2) analytical methods. In all cases, the uncertainties associated with structural modeling, material properties, loading condition, etc. are captured using a variety of techniques that rely on probabilistic or fuzzy treatment of random variables.

Prevalent among the random sampling methods are the traditional Monte Carlo simulation and its variants such as adaptive importance sampling (e.g., Wu 1994) and robust importance sampling (e.g., Torng *et al.* 1996). These methods have been developed to reduce the simulation cycles by adjusting the sampling domain to the important region near the most probable point (MPP) of failure.

Analytical methods such as the first- and second-order reliability methods (FORM and SORM) are based on the formulation of the limit state function that defines the surface separating the failure and safe regions of the design space. These techniques are used to determine the reliability (safety) index represented by the shortest distance from the origin of the reduced coordinate system to the limit state surface. A commonly used procedure for the calculation of safety index is that developed by Hasofer and Lind (1974) and expanded by Rackwitz and

Fiessler (1978) to include the effect of distribution type as well as the mean value and standard deviation of each random variable.

The calculations of reliability index as well as the probability of failure often require repeated evaluations of the limit state function as a result of perturbations in the random variables in search of MPP. This repeated evaluation of the limit state function and its sensitivity derivatives are highly dependent on the complexity and computational intensity of the underlying failure analysis as well as the number and distribution type of random variables considered. In order to reduce this computational burden, it is possible to develop an accurate analytical model as a surrogate for the more exact failure analysis. This approach is made possible with the help of response surface methodology (RSM).

Bucher and Bourgund (1990) used an adaptive interpolation scheme to represent the system behavior by a response surface (RS) model, which was then combined with importance sampling to obtain the desired reliability estimates. Liu and Moses (1994) combined the sequential RSM with Monte Carlo importance sampling to develop a reliability analysis program for aircraft structural systems; whereas, Liaw and DeVries (2001) developed a reliability-based optimal design process by integrating reliability and variability analyses with optimization design processes using RSM.

The research presented in this report examines the use of RSM in reliability-based optimization of composite structures through the development of two alternative strategies, one dubbed the global response surface technique (GRST) and the other sequential local response surface technique (SLRST).

These two strategies are applied in RBO of a thin-walled composite circular cylinder under axial compression with the results used to compare the accuracy and efficiency of these techniques.

The remainder of this report is organized as follows. In Section 2 a brief overview of structural reliability is presented. This is followed by a detailed discussion of the RBO example problem in Section 3, which includes the description of GRST and SLRST and corresponding results. Reliability sensitivity analysis results are presented in Section 4 followed by the concluding remarks in Section 5. The description of the shell buckling analysis is given in Appendix A while that for the selection of design points for SLRST implementation is given in Appendix B.

2. Overview of structural reliability

In its fundamental form, the probability of failure of a structural component may be expressed as

$$P_f = P\left(g(X) \leq 0\right) \tag{1}$$

where $X = \left\{X_1, X_2, ..., X_n\right\}^T$ is an n-dimensional vector of random variables and $g(X)$ is the limit state function describing the failure criterion, such that $g < 0$ represents failure, $g > 0$ represents safety, and $g = 0$ represents the limit state surface separating the safe and failed regions. The

failure probability is found by evaluating the multiple integral of the joint probability density function $f_X(\boldsymbol{x})$ over the failure region, Ω expressed as

$$P_f = \int\int...\int_{\Omega} f_X(x_1, x_2, ..., x_n)dx_1dx_2...dx_n \tag{2}$$

For problems involving multiple random variables, the integration of $f_X(\boldsymbol{x})$ is in general very difficult. Hence, the probability of failure is usually estimated using variety of approximation techniques including those commonly known as the random sampling methods (e.g., Monte Carlo simulation), analytical methods (e.g., FORM), or hybrid methods (e.g., AMV+ combined with AIS, Wu 1994).

In applying the standard time-invariant FORM, the limit state $g(\boldsymbol{X})$ is transformed to standard normal space $g(\boldsymbol{u})$ with MPP found by solving the optimization problem

$$\begin{aligned} &\text{Min} \quad \left|\boldsymbol{u}^*\right| = \sqrt{\boldsymbol{u}^T\boldsymbol{u}} \\ &\text{S. T.} \quad g(\boldsymbol{u}) = 0 \end{aligned} \tag{3}$$

where the distance to MPP is defined as the reliability or safety index $\beta = \left|\boldsymbol{u}^*\right|$, which is then used to estimate the probability of failure (for $\beta > 0$) as

$$P_f \approx \Phi(-\beta) \tag{4}$$

where Φ is the cumulative distribution function of a standard normal random variate

The optimization problem in Eq. (3) may be solved using a variety of mathematical programming techniques such as that developed by Shinozuka (1983) or other more tailored techniques including those developed by Hasofer and Lind (1974) and extended by Rackwitz and Fiessler (1978) to problems involving non-normal random variables. In this research, we used the standard time-invariant FORM to find β.

One advantage of analytical over simulation-based techniques is that they facilitate the calculation of probabilistic sensitivity factors represented by the partial derivatives of β with respect to the mean and standard deviation of random variable X_i as (Madson et al. 1986)

$$\frac{\partial\beta}{\partial\mu_{X_i}} = \left(\frac{\partial\beta}{\partial u_i}\right)\left(\frac{\partial u_i}{\partial\mu_{X_i}}\right) \tag{5-a}$$

$$\frac{\partial\beta}{\partial\sigma_{X_i}} = \left(\frac{\partial\beta}{\partial u_i}\right)\left(\frac{\partial u_i}{\partial\sigma_{X_i}}\right) \tag{5-b}$$

While the sensitivity factors in Eq. (5-a) can help measure the influence of each random variable on β, those in Eq. (5-b) quantify the effect of parametric uncertainty on component reliability.

3. Reliability-based structural optimization problem

The goal of RBO is to achieve structural efficiency while fulfilling the requirement for safety. In this regard, parameters with uncertainty are treated as probabilistic random variables with each defined by its mean value, standard deviation, and probability distribution. Additionally, each failure constraint is formulated in terms of probability of failure or the corresponding safety index.

The design problem considered here is a thin-walled circular cylinder under uniform axial compression as shown in Fig. 1, with the loaded edges clamped.

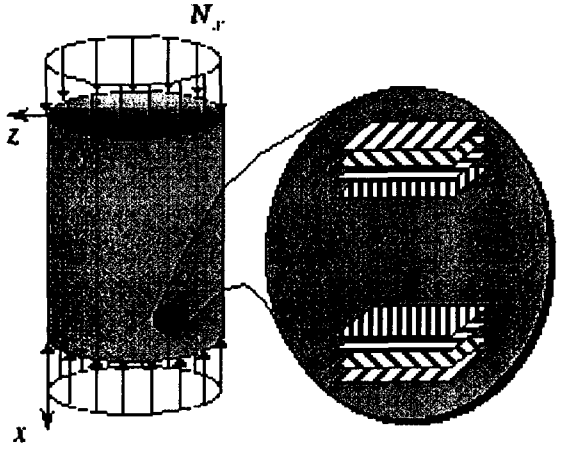

Fig. 1 Structural model of thin-walled composite cylinder and loading condition

The cylinder wall consists of a 16-layer symmetric laminate with each layer made of unidirectional carbon/epoxy tape with statistical properties shown in Table 1. In addition to the material properties, the thickness and orientation angle of each layer on one side of the plane of symmetry are also treated as independent random variables with the mean thickness in layers 1 through 8 treated as design variables. The cylinder length (L) and inner diameter (D) are allowed to have three specific mean values as indicated in Table 1. Completing the list of random variables is the resultant axial load, P_a. In this problem, all random variables have normal distribution with assumed coefficients of variation (COV) given in Table 1.

The RBO problem in this example is formulated as

$$\begin{aligned} &\text{Min} \quad E[W(X)] \\ &\text{S.T.} \quad \beta_b \geq \beta_{\min} \\ &\text{and} \quad Y_i^l \leq Y_i \leq Y_i^u, \qquad i = 1,2,...,8 \end{aligned} \tag{6}$$

where the objective function represents the expected or mean cylinder weight and β_b represents the reliability index associated with axial buckling load, which is assumed to be the only mode of failure with the method of analysis described in Appendix A. The target component reliability index is denoted by β_{min}. The design variables Y_1 through Y_8 correspond to a subset of random variable vector, X and are constrained by their respective lower and upper bounds. Although the COV of each ply thickness is held fixed, the corresponding standard deviation is subject to change during the optimization process as a result of changes in mean ply thicknesses (i.e., design variables).

Table 1 Statistical properties of random variables

Random Variable No.	Definition	Unit	Mean Value	COV (%)
1	E_1	psi	18.0e6	1.33
2	E_2	psi	1.35e6	1.67
3	ν_{12}	—	0.226	2.0
4	G_{12}	psi	0.543e6	2.0
5-12	t_{ply}	in	$[Y_1 / Y_2 / ... / Y_8]$	5.0
13-20	θ_{ply}	deg	$[\theta_1 / \theta_2 / ... / \theta_8]$	σ_θ [a]
21	D	in	$10 \le E[D] \le 20$	5.0
22	L	in	$10 \le E[L] \le 20$	5.0
23	P_a	lb	0.10e6	5.0

[a]Standard Deviation

The optimization problem in Eq. (6) is solved using the method of sequential quadratic programming in the optimization software, DOT (1999) based on two alternative strategies for evaluation of β_b. As will be described in the following section, these strategies take advantage of response surface methodology to increase the efficiency of component reliability evaluation, which is the most time-consuming part of reliability-based design optimization process for the types of problem such as the one considered here.

3.1 Global response surface technique (GRST)

In applying GRST, a single second-order RS model in n factors expressed as

$$\hat{P}_{cr}(X) = a_0 + \sum_{i=1}^{n} a_i X_i + \sum_{i=1}^{n} \sum_{j=1}^{i} a_{ij} X_i X_j \tag{7}$$

and denoted as the global response surface model (GRSM) is used to estimate the axial buckling force, P_{cr} over the entire feasible design space. This is done in lieu of calculating the "exact" P_{cr} from a more costly buckling analysis described in Appendix A. Equation (7) is a fully quadratic model with $(n+1)(n+2)/2$ coefficients. With the cylinder axial buckling affected by random variables 1 through 22 in Table 1, Eq. (7) will be a function of 22 factors for a total of 276 unknown coefficients.

To evaluate the buckling reliability index, β_b using FORM, we approximate the limit state function as

$$g(X) \approx \hat{g}(X) = \hat{P}_{cr} - P_a \tag{8}$$

where $\hat{P}_{cr}$ is calculated from Eq. (7) and P_a, representing the applied axial force, is defined as random variable X_{23}. Since $\hat{g}(X)$ is a nonlinear function of random variables, the evaluation of β_b becomes an iterative process within the RBO Solution block in the flowchart of optimization procedure shown in Fig. 2.

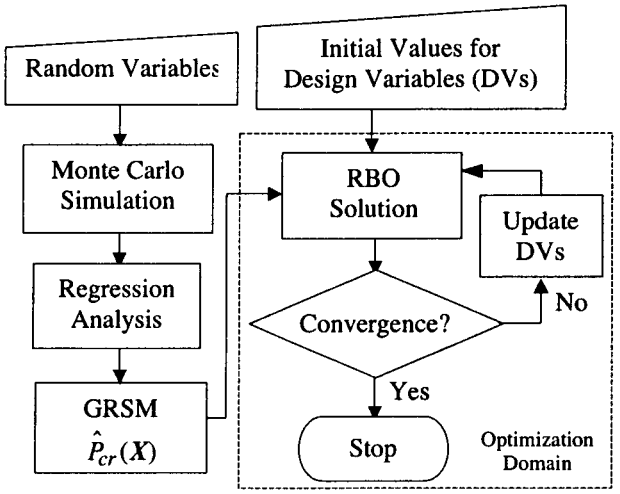

Fig. 2 Flowchart of optimization procedure with GRST

Thus, the main challenge in implementation of GRST is the development of an accurate GRSM for $\hat{P}_{cr}$. For generating the necessary response population in fitting a second-order RS model commonly used methods include experimental design (e.g., central composite design, Box-Behnken) and random sampling (e.g., Latin Hypercube). In this problem we used the method of least squares to estimate the unknown coefficients in Eq. (7) based on a population of response samples generated using Monte Carlo simulation (MCS), which is more robust but somewhat less efficient than the stratified random sampling and some of the available experimental design methods.

In performing MCS, we assumed each random variable has a uniform distribution with the corresponding lower and upper limits found as

$$X_j^u,\ X_j^l = (1 \pm \varsigma_{X_j})\mu_{X_j}, \qquad j = 1,2,...,n \tag{9}$$

where ς_{X_j} represents the bound increment (BI) on ith random variable with all values shown in Table 2. The values of BI for material properties extend the range of GRSM to a minimum of $\mu \pm 3\sigma$ for each property. The large BI for ply thickness set the min and max values to 0.0025

in. and 0.0075 in. For $\theta_{ply} \neq 0$, the selected BI extends the domain of GRSM by considering variability and uncertainty in ply orientation angle. Finally, the large BIs for length and diameter allow the use of GRSM for the range of cylinders identified in Table 1.

Table 2 Bound increments on random variables

Random Variable	ς_{X_j} (%)
E_1	4
E_2	5
ν_{12}	6
G_{12}	6
t_{ply}	50
θ_{ply}	26
D	50
L	50

A deterministic computer program based on the procedure described in Appendix A is used to calculate the "exact" buckling load with the 12th degree Legendre polynomial as the interpolation function. Each analysis run takes approximately one minute and fifteen seconds of CPU time on a 900MHz Sun Fire 480R. For the subsequent numerical analyses, we considered a cylinder with mean ply angles and laminate stacking sequence specified as $(\pm 45 / 90_4 / \mp 45)_s$.

For response surface analysis, we defined Eq. (7) as a multiple linear regression model with the least-squares approximations of the unknown coefficients found using a combination of GLMMOD and REG procedures in SAS version 8.0.

Several candidate models based on increasing number of response samples were developed and compared prior to selecting the most appropriate GRSM for reliability-based optimization. The results of statistical analysis are summarized and shown in Table 3 with the last two rows in the table showing the results for a linear model (i.e., 3000L) and that excluding all the interaction terms (i.e., 3000LQ).

In terms of RMSE adjusted R^2, and COV, the model based on 500 samples appears to have a slight advantage over the rest. However, according to Freund and Littell (2000), the presence of significant round-off errors could cause the predicted residual sum of squares (PRESS) to be drastically different from the sum of squares of actually computed residuals (SS Error). In this case, this ratio is very large for the 300-sample case but quickly drops as the sample size is increased. The results in the last two rows indicate that in this problem, the interaction terms are very important and their exclusion would greatly compromise the accuracy of the resulting RS model as indicated by the much larger RMSE value.

In addition to the statistics shown in Table 3, we also used the variance inflation factor (VIF) to detect the presence of multicollinearities among the 22 independent variables. In this case, the VIF values were found to be in the range of 1.003 to 1.012 indicating no multicollinearities among the independent factors.

The plots of studentized residuals and actual buckling load responses versus the predicted buckling loads for the fully quadratic RS model are shown in Fig. 3.

Table 3 Comparison of candidate models for GRST

Sample Size	Sample Mean	RMSE	R^2	Adj. R^2	COV(%)	PRESS/ SS Error
300	145372	4684.0	0.998	0.976	3.22	194.0
500	143275	4379.0	0.991	0.979	3.06	5.6
1000	143089	4794.8	0.981	0.974	3.35	2.0
1500	143019	4907.9	0.978	0.973	3.43	1.6
2000	143413	4895.1	0.977	0.974	3.41	1.4
2500	143337	4967.2	0.976	0.973	3.47	1.3
3000	143030	4939.7	0.976	0.973	3.45	1.2
3000L	143030	9464.0	0.902	0.901	6.62	1.02
3000LQ	143030	8897.5	0.914	0.912	6.22	1.03

The search for influential observations through the use of Cook's D and Hat Diagonal did not indicate the presence of any outliers.

To complete the examination of candidate RS models, each model was tested for accuracy based on its predictability of buckling response at design points not included in the multiple linear regression modeling. In this case, a set of 50 design points was generated using Latin Hypercube Sampling (LHS) feature of VisualDOC (2002) with the exact and predicted buckling loads evaluated at each design point. Table 4 gives a summary of results found in this examination.

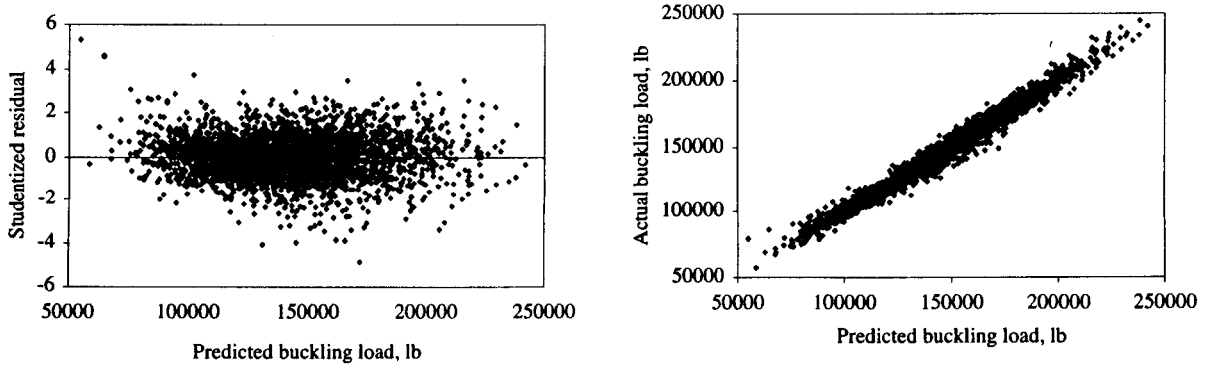

(a) (b)

Fig. 3 Plots of studentized residual (a) and actual buckling load (b) for the GRSM based on 3000 response samples

These results indicate no statistical difference between the exact mean and the approximate mean predicted by each candidate GRS model. Although, in terms of maximum residual, the 3000-sample model performs the best, there is no significant difference among the models beyond 1000 samples; therefore, any of these models would be an acceptable candidate for GRST. Upon considering all the available information, we opted to use the model based on 3000 response samples for GRST-based solution of the RBO problem.

Table 4 Predictability of candidate GRS models

Model	P_{cr}, lb	ε_{max}, lb	ε_{ave}, lb
Exact	138535	—	—
500	139684	22569	6713
1000	139163	12361	4228
1500	138260	12001	4537
2000	139984	12357	4652
2500	139902	12225	4738
3000	139423	11739	4651

A computer program based on the procedure described in Fig. 2 was developed to obtain the solutions for the RBO problem. The results presented in Table 5 below are based on the following conditions: Mean ply angles $(\theta_1 / ... / \theta_8)_s = (\pm 45 / 90_4 / \mp 45)_s$; Ply angle standard deviation σ_{θ_i} = 3 deg.; Side constraints Y_i^l =0.0029 in., Y_i^u =0.0065 in.; Initial values of design variables, Y_i = 0.005 in.; Three combinations of mean length and diameter; Two different values for COV of the applied load; Target reliability: β_{min} = 3.72 (i.e., P_f = 0.0001)

The quantities shown are the mean values for the estimated buckling load, $\hat{P}_{cr}$, cylinder weight, W, and cylinder wall thickness, h.

Table 5 RBO results using GRST

	Mean value at optimum design	
Parameter	COV(P_a) = 5%	COV(P_a) = 10%
Mean diameter = Mean length =10 in.		
$\hat{P}_{cr}$, lb	124,537	141,517
W, lb	1.31	1.40
h, in	0.0724	0.0778
Mean diameter = 10 in., Mean length = 20 in.		
$\hat{P}_{cr}$, lb	128,560	143,969
W, lb	2.73	2.92
h, in	0.0757	0.0808
Mean diameter = 20 in., Mean length = 10 in.		
$\hat{P}_{cr}$, lb	126,016	142,396
W, lb	2.57	2.75
h, in	0.0715	0.0765

The effect of uncertainty in the applied load is illustrated through the use of two different COV values (i.e., 5% and 10%).

3.2 Sequential local response surface technique (SLRST)

Although GRST provides considerable computational time saving by eliminating repeated exact buckling analyses in the evaluation of β_b and the solution of RBO problem, it still requires a rather large number of simulation cycles for development of an accurate GRSM at pre-

optimization stage. A potentially more efficient alternative to GRST is the sequential local response surface technique (SLRST).

In SLRST, the design space is partitioned into smaller subregions and in each subregion a linear RS model (LRSM) in the form

$$\tilde{P}_{cr}(\boldsymbol{X}) = a_0 + \sum_{i=1}^{n} a_i X_i \tag{10}$$

is used to approximate the axial buckling force.

Inspired by the sequential local approximate optimization technique, the procedure for SLRST, shown in Fig. 4, is similar in principle to the multipoint approximation method of Toropov et al. (1993) and Polykin et al. (1995), and the sequential local optimization strategy implemented by Sevant et al. (2000).

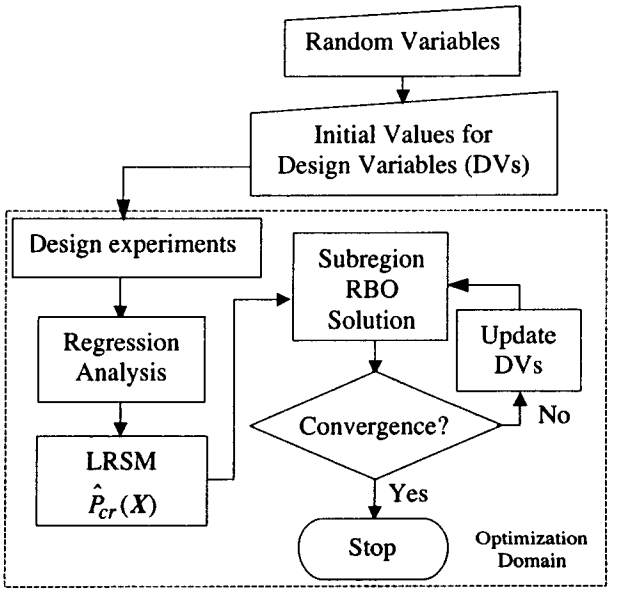

Fig. 4 Flow chart of the optimization procedure using SLRST

The main advantage of SLRST is that since the limit state function is described by a linear equation, the reliability index can be calculated using the basic reliability formula

$$\beta_b = \frac{\mu_{\hat{P}_{cr}} - \mu_{P_a}}{\sqrt{\sigma^2_{\hat{P}_{cr}} + \sigma^2_{P_a}}} \tag{11}$$

where $\mu_{\hat{P}_{cr}}, \mu_{P_a}$ are the mean values of $\hat{P}_{cr}$ and P_a, respectively, and $\sigma_{\hat{P}_{cr}}, \sigma_{P_a}$ are the corresponding standard deviations with the variance of $\hat{P}_{cr}$ determined as

$$\sigma^2_{\hat{P}_{cr}} = \sum_{i=1}^{n} \left(\frac{\partial \hat{P}_{cr}}{\partial X_i} \right)^2 \sigma^2_{X_i} = \sum_{i=1}^{n} a_i^2 \sigma^2_{X_i} \tag{12}$$

where the partial derivatives of $\hat{P}_{cr}$ are found analytically from the LRSM.

Because in SLRST, a separate LRSM is developed for each subregion optimization, the overall efficiency of this approach is governed by how efficiently the unknown coefficients of each LRSM are calculated.

With 22 random variables, Eq. (10) has a total of 23 unknown coefficients. Theoretically, only 23 design points and corresponding response values are needed for the calculation of the unknown coefficients. However, is it possible to find a reasonably accurate LRSM with only 23 response observations? Furthermore, does the accuracy of LRSM depend on how the design points are selected?

To answer these questions, we conducted a preliminary study by developing six separate LRS models based on six different experimental and random design approaches (i.e., Koshal, Box-Behnken, Taguchi, Latin Hypercube Sampling, Random, and Quadrature).

The Random design points are obtained using a random number generator while the Quadrature design points are found using the non-uniformly spaced quadrature formulae described in Appendix B. Overall, Taguchi and Box-Behnken require 81 and 44 design points, respectively, while the remaining four approaches require only 23.

Table 6 shows the listing of random variables, their mean values as well as the corresponding lower and upper bounds used in developing the six candidate LRS models. The lower and upper bounds in Table 6 are found using the quadrature formulae in Appendix B and could be interpreted as those defining a single subregion in SLRST implementation.

With the exception of Quadrature design, the design points for other approaches were obtained using VisualDOC (2002). Furthermore, the unknown coefficients in all LRS models were obtained using the REG procedure of SAS.

To examine their accuracy, we used each candidate LRSM, defined in Table 7, to calculate the buckling load with all random variables kept at their respective mean values. These results are shown in column 2 of Table 8. In addition, we generated 25 random design points (other than those used in developing any of the LRS models but consistent with the bounds in Table 6) and calculated the response value at each location using the six LRS models. Columns 3 and 4 in Table 7 show the maximum and average residuals for each model with the ratio of average error to exact mean buckling load shown in column 5.

It is clear from these results that the selection of design points does make a difference in the accuracy of the resulting LRSM as Taguchi, Box-Behnken, and Quadrature designs produced more accurate models than the rest. However, in terms of efficiency, the Quadrature design is the most superior, as it requires only 23 design experiments compared to 81 for Taguchi and 44

for Box-Behnken. Therefore, based on these findings, the Quadrature design was subsequently adopted for the SLRST-based solution to the RBO problem.

Table 6 Bounds on random variables according to the quadrature formulae in Appendix B

Random Variable	Mean Value	Lower Bound	Upper Bound
E_1, psi	1.800E+07	1.795E+07	1.912E+07
E_2, psi	1.350E+06	1.345E+6	1.456E+06
ν_{12}	0.226	0.225	0.247
G_{12}, psi	5.430E+05	5.403E+05	5.939E+05
t_1, in	0.005	0.0049	0.0061
t_2, in	0.005	0.0049	0.0061
t_3, in	0.005	0.0049	0.0061
t_4, in	0.005	0.0049	0.0061
t_5, in	0.005	0.0049	0.0061
t_6, in	0.005	0.0049	0.0061
t_7, in	0.005	0.0049	0.0061
t_8, in	0.005	0.0049	0.0061
θ_1, deg	45.0	40.8	58.7
θ_2, deg	-45.0	-48.2	-31.4
θ_3, deg	90.0	87.4	103.6
θ_4, deg	90.0	87.4	103.6
θ_5, deg	90.0	87.4	103.6
θ_6, deg	90.0	87.4	103.6
θ_7, deg	-45.0	-48.2	-31.4
θ_8, deg	45.0	40.8	58.7
D, in	20.0	18.0	24.0
L, in	10.0	8.3	11.7

An example of the sequence of subregion optimization is depicted in Fig. 5 with the initial design pointed designated by S. With COV of each ply thickness held fixed, the size of each subregion is determined based on the subregional (local) lower and upper bounds on the design variables defined as

$$Y_{i,k}^{l,u} = Y_{i,k} \mp \delta_{i,k}^{l,u} \qquad i = 1,2,...,8 \tag{13}$$

where $Y_{i,k}$ is the value of ith design variable at the beginning of kth subregion optimization cycle with the corresponding lower and upper move limits calculated as

$$\delta_{i,k}^{l} = Y_{i,k}\left(COV(t)\sqrt{\frac{n+1}{(n-10)(n-11)}} \right) \tag{14-a}$$

$$\delta_{i,k}^{u} = Y_{i,k}\left(COV(t)\sqrt{\frac{(n+1)(n-11)}{(n-10)}} \right) \tag{14-b}$$

Table 7 Coefficients in each candidate LRSM

Random Variable	RS Coefficient	Koshal	B-B	Taguchi	LHS	Random	Quadrature
—	a_0	-62107.69	-191034.77	-188337.22	806970.26	-422810.24	-250237.00
E_1	a_1	0.006402	0.008339	0.006432	-0.066344	0.014638	0.008319
E_2	a_2	0.011382	0.015254	0.006039	0.143120	-0.007214	0.026950
ν_{12}	a_3	5909.09	6818.18	-319.87	6517713.61	-156591.33	85139.52
G_{12}	a_4	0.024231	0.0328	0.021983	-2.2865	0.012186	0.058529
t_1	a_5	5730769	7446154	8329630	12846767	13073274	7366942
t_2	a_6	9800000	11161538	10094302	-11496414	11840124	10705970
t_3	a_7	7276923	9069231	7733333	-16173878	1542889	8878919
t_4	a_8	7276923	9069231	7118234	7367939	10791940	8987386
t_5	a_9	7276923	9069231	7927350	-18894534	-67322	9107382
t_6	a_{10}	7276923	9069231	8138177	26805393	-10111602	9246309
t_7	a_{11}	5476923	6000000	7515385	74168144	6383828	7808193
t_8	a_{12}	6161538	6753846	8390313	36139560	16876669	8444851
θ_1	a_{13}	-1119.55	-1086.59	-1148.46	2111.13	-323.175	-1093.78
θ_2	a_{14}	1032.14	1706.55	1320.66	-1048.38	872.72	1034.13
θ_3	a_{15}	-350.000	-239.506	-68.930	-1302.09	455.058	-280.605
θ_4	a_{16}	-387.037	-251.235	-121.491	1033.4	-66.6697	-301.852
θ_5	a_{17}	-417.901	-259.877	-122.634	1106.4	288.169	-315.524
θ_6	a_{18}	-441.975	-268.519	-159.694	-4298.37	604.96	-320.028
θ_7	a_{19}	223.214	167.857	14.3078	-3174.94	587.593	68.8512
θ_8	a_{20}	337.989	482.682	206.683	1031.57	1399.56	162.724
D	a_{21}	18.3333	-608.333	105.062	-20840.49	-1387.45	-318.352
L	a_{22}	2029.41	2802.94	1572.88	-123.604	1193.18	2069.58

The 8 thickness design variables correspond to the mean values of random variables 5 through 12. In that group, the twelfth random variable has the smallest perturbations away from the mean according to Quadrature design (see Appendix B). Therefore, the move limits in Eq. (14) are specified based on perturbations in the twelfth random variable.

Table 8 Comparison of candidate LRS models

	$\mu_{P_{cr}}$ lb	ε_{max}, lb	ε_{ave}, lb	$\varepsilon_{ave}/P_{cr_{exact}}$
Exact	1.543e5	—	—	—
Koshal	1.497e5	2.17e4	8.58e3	4.6%
B-B	1.498e5	1.72e4	5.34e3	2.9%
Taguchi	1.465e5	1.21e4	4.27e3	2.3%
LHS	1.932e5	1.76e5	8.25e4	44.4%
Random	1.361e5	2.93e4	1.27e4	6.8%
Quadrature	1.528e5	1.22e4	6.00e3	3.2%

For COV(t) = 5% and n = 22, we find $\delta_{i,k}^{l} = 0.02087\, Y_{i,k}$ and $\delta_{i,k}^{u} = 0.22958\, Y_{i,k}$, which indicate unsymmetric move limits with more than a 10 to 1 ratio favoring freedom of movement towards

the upper bound. If at the end of kth subregion optimization cycle, design variables have different values, then they will be subject to different move limits in cycle k+1.

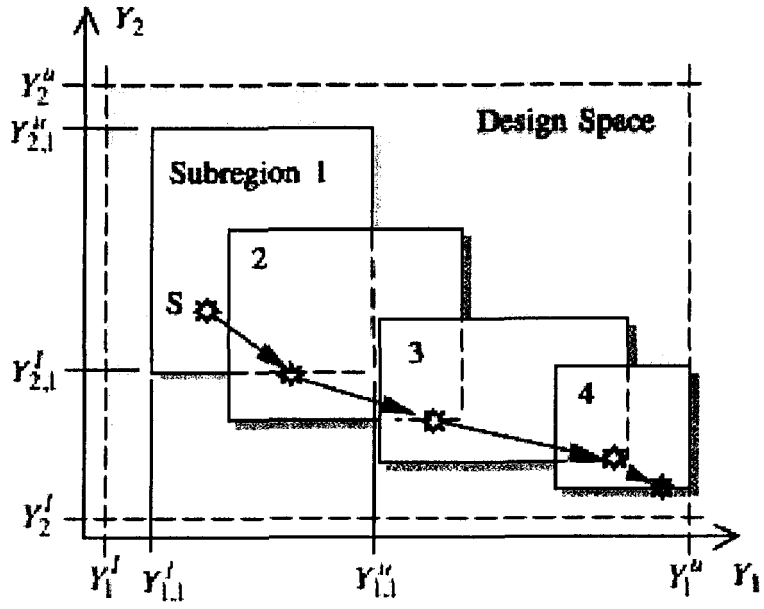

Fig. 5 A notional schematic of SLRST over four subregions for a 2-dimensional design space

By staying within the specified move limits, the buckling load estimates obtained from LRSM are found to be fairly accurate with an observed error of no more than roughly 1.5 to 2%.

With the local bounds defined, design improvement is sought in the current subregion by solving the mathematical programming problem in Eq. (6). Upon completion of one subregion optimization cycle, the search continues to the next cycle focusing on an updated subregion with location defined by the final values of design variables in the current subregion and its size determined by Eqs. (13) and (14).

The move limits are reduced in half if the absolute difference between objective functions in two consecutive cycles is less than $6\text{x}10^{-4}$, and hard convergence is reached when the difference is less than or equal to $6\text{x}10^{-6}$.

The SLRST-based optimization results for the same cylinder geometry, loading conditions, and target reliability as in Table 5 are shown in Table 9.

These results are based on an initial mean ply thickness (design variable) of 0.004 in. From this initial design, it takes an average of 10 subregion optimization cycles to reach optimal design. Because of unsymmetric move limits, the choice of initial design can influence the number of subregion optimization cycles performed. To demonstrate this characteristic, the convergence history for E[D]/E[L]/COV(P_a) = 20/10/10 cylinder with two different initial design points is shown in Fig. 6. Curve A is for the initial mean ply thickness of 0.006 in. while Curve B is for 0.004 in.

Table 9 RBO results using SLRST

Parameter	Mean value at optimum design	
	$COV(P_a) = 5\%$	$COV(P_a) = 10\%$
Mean diameter = Mean length =10 in.		
$\hat{P}_{cr}$, lb	129463	142953
W, lb	1.33	1.42
h, in	0.0737	0.0789
Mean diameter = 10 in., Mean length = 20 in.		
$\hat{P}_{cr}$, lb	129375	145163
W, lb	2.78	2.96
h, in	0.0771	0.0821
Mean diameter = 20 in., Mean length = 10 in.		
$\hat{P}_{cr}$, lb	132311	147664
W, lb	2.63	2.79
h, in	0.0732	0.0776

Since the thickness in each ply is treated as an independent random variable, it is possible for the plies that have the same mean orientation angles to have different thickness values. Figure 7 shows the variation in the eight design variables from initial to final point corresponding to Curve B in Fig. 6.

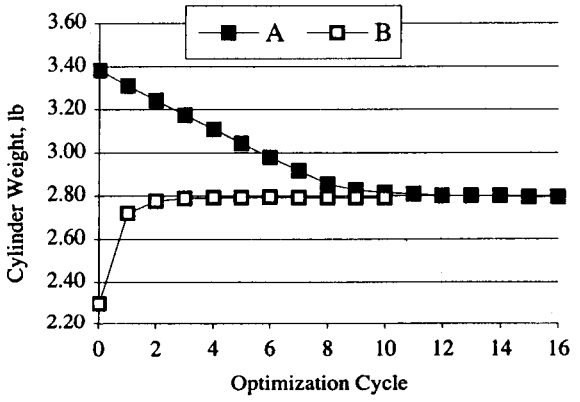

Fig. 6 Convergence history based on two different initial design points

To validate the accuracy of our reliability analysis and to determine whether the optimal design meets the specified target reliability index and probability of failure, we performed an independent analysis using the structural reliability code, NESSUS (2002). Because of its reasonably good efficiency and accuracy, we chose the analytical method AMV+ for reliability index and probability of failure calculations. In this case, NESSUS calls the exact buckling analysis code directly for each limit state function evaluation and has no interaction with any of the RS models developed here. Table 10 shows the reliability index and probability of failure values for the optimal designs obtained through SLRST.

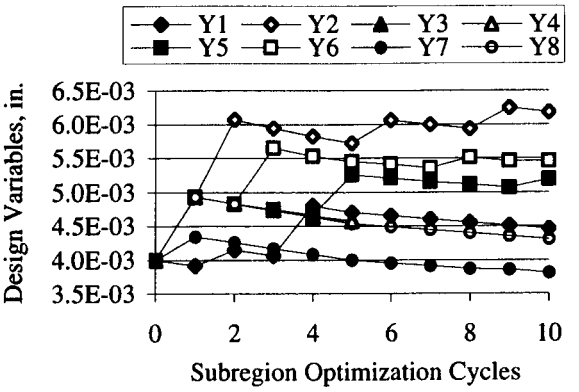

Fig. 7 Convergence history of design variables for the cylinder with E[D]/E[L]/COV(P_a) = 20/10/10

To measure the effect of ply pattern on optimal design, SLRST was used to obtain optimal design solutions for cylinders with four different mean ply orientation angles. The results shown in Table 11 are for the E[D]/E[L]/COV(P_a) = 20/10/10 cylinder with target reliability index of 3.72 and mean ply orientation angles and stacking sequence as follows: PP1: $(\pm 45 / 90_4 / \mp 45)_s$; PP2: $(\pm 45 / 0_4 / \mp 45)_s$; PP3: $(\pm 45 / 0 / 90)_{2s}$; PP4: $(0 / \pm 30 / \pm 45 / \pm 60 / 90)_s$

Table 10 Comparison of structural reliability estimates at COV(P_a) = 10%

Parameter	SLRST	NESSUS
Mean diameter = Mean length =10 in.		
β	3.72	3.78
P_f	1.0e-4	0.78e-4
Mean diameter = 10 in., Mean length = 20 in.		
β	3.72	3.63
P_f	1.0e-4	1.4e-4
Mean diameter = 20 in., Mean length = 10 in.		
β	3.72	4.16
P_f	1.0e-4	0.16e-4

Table 11 SLRST-based RBO results for cylinders with various mean ply patterns

Parameter	PP1	PP2	PP3	PP4
$\tilde{P}_{\sigma}$, lb	147664	146653	146320	148682
W, lb	2.79	2.87	2.59	2.56
h, in	0.0776	0.0799	0.0720	0.0712

Figure 8 shows the convergence history for the designs in Table 11 with the optimal mean ply thickness values shown in Table 12.

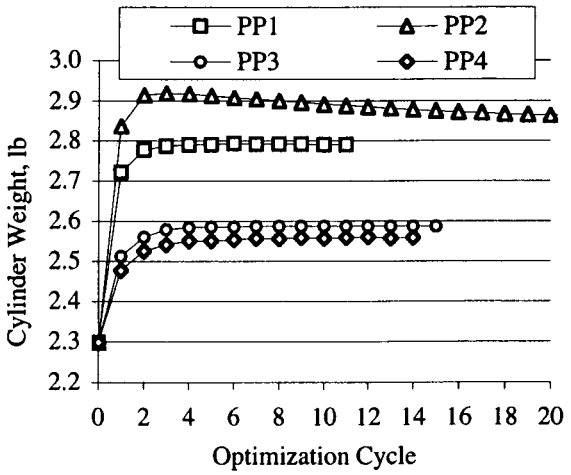

Fig. 8 Convergence history for cylinders with four different ply patterns

Table 12 SLRST-based RBO results for cylinders with various mean ply patterns

Mean Ply Thickness	PP1	PP2	PP3	PP4
t_1, in	4.4E-03	3.3E-03	3.3E-03	3.6E-03
t_2, in	6.2E-03	3.3E-03	4.3E-03	3.6E-03
t_3, in	4.6E-03	4.7E-03	4.0E-03	4.3E-03
t_4, in	4.9E-03	4.9E-03	4.4E-03	5.3E-03
t_5, in	5.2E-03	5.2E-03	4.9E-03	4.4E-03
t_6, in	5.5E-03	5.4E-03	5.2E-03	5.0E-03
t_7, in	3.9E-03	6.5E-03	5.0E-03	4.5E-03
t_8, in	4.2E-03	6.5E-03	5.1E-03	4.9E-03

The SLRST and GRST-based solutions are comparable in terms of accuracy. However, in terms of computational efficiency, the two techniques are considerably different. While in GRST, the number of exact buckling response evaluations is independent of the number of optimization iterations, in SLRST it is not, as each subregion optimization cycle requires 23 exact buckling load evaluations. Depending on the model used, GRST required from 1000 to 3000 design points and exact buckling response evaluations as indicated in Tables 3 and 4. By contrast, the number of design points and responses required by SLRST was 23 times the number of optimization cycles, which varied from a minimum of 3 to a maximum of 20 for a total of 69 to 406, respectively.

4. Reliability Sensitivity Analysis

The probabilistic sensitivity derivatives of reliability index in Eq. (5) are evaluated at the design point x^* and normalized as

$$\delta_i = \frac{\partial \beta_b}{\partial \mu_{X_i}}\bigg|_{x^*} \left(\frac{\mu_{X_i}}{\beta_b}\right), \qquad i = 1,2,...,n \tag{13-a}$$

$$\eta_i = \left.\frac{\partial \beta_b}{\partial \sigma_{X_i}}\right|_{x^*} \left(\frac{\sigma_{X_i}}{\beta_b}\right), \qquad i = 1,2,\ldots,n \tag{13-b}$$

and plotted in Fig. 9 for a composite cylinder with $(\pm 45 / 90_4 / \mp 45)_s$ mean ply pattern and E[D]=E[L]=15 in. In this case, the GRSM is used for the evaluation of the sensitivities.

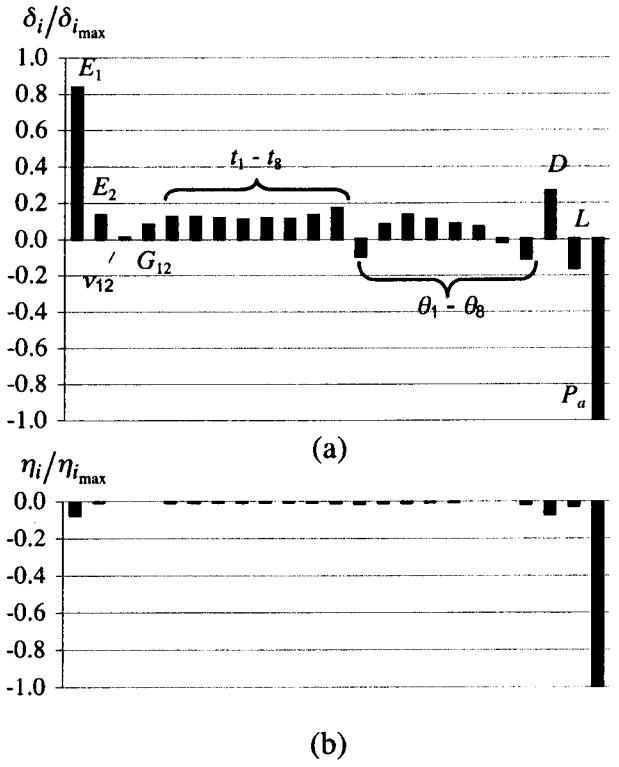

Fig. 9 Normalized sensitivity derivatives of β_b with respect to the mean (a) and standard deviation (b) of each random variable

Of all random variables, the applied load is found to have the greatest influence on β_b followed by elastic modulus in fiber direction and cylinder diameter.
Although total shell thickness has a large impact on P_{cr}, the influence of each individual ply thickness is less significant.

As for the effect of parametric uncertainty, it is evident from Fig. 9-b that the amount of scatter in the applied load has the largest effect on β_b. Without the sensitivity derivatives of β_b with respect to P_a, Fig. 9 is replaced by Fig. 10, which more clearly shows the influence of random variables on β_b through P_{cr}.

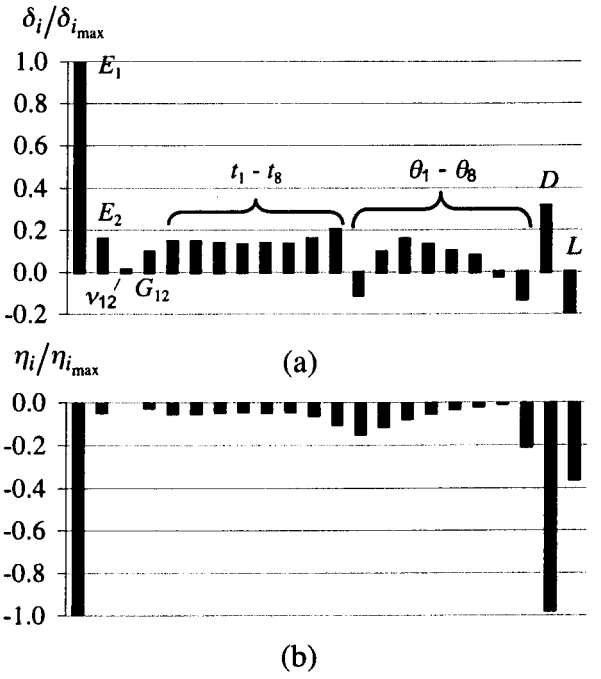

Fig. 10 Normalized sensitivity derivatives of β_b with respect to the mean (a) and standard deviation (b) of random variables affecting P_{cr}

5. Concluding remarks

This report presented the development of global and sequential local response surface techniques for reliability-based optimization of composite structures. These techniques were subsequently applied to reliability-based optimization of a composite circular cylinder under axial compression and buckling instability.

Based on the formulation and solution of the cylinder RBO example problem, the following conclusions are reached:

- As in most RBO problems, the computational requirement for reliability index evaluation far exceeds that for design space search of optimal point.
- RBO results using GRST and SLRST have the same level of accuracy.
- SLRST has a superior computational efficiency than GRST as in most cases it required 5 to 10 times fewer exact buckling response evaluations.
- The choice of experimental design technique affects the accuracy and efficiency of LRS models with the Quadrature design found to be most efficient.
- The non-uniformly spaced quadrature formulae result in greater freedom of movement toward the upper than the lower bound in each subregion optimization. This could speed up or slow down the search toward optimal design depending upon the choice of initial design point.
- Among all random variables, the applied load followed by elastic modulus in the fiber direction and diameter were found to have the greatest influence on cylinder reliability index.

- Besides the mean value, the amount of scatter in applied load is found to have a large influence on cylinder reliability and optimal cylinder wall thickness.
- The choice of laminate ply pattern affects cylinder reliability through changes in the buckling load.

References

Ayyub, B. M.; McCuen, R. H. 1997: *Probability, Statistics, & Reliability for Engineers.* Boca Raton: CRC Press, pp. 404-408

Bucher, C.G.; Bourgund, U. 1990: A fast and efficient response surface approach for structural reliability problems. *Structural Safety* **7**, 57-66

DOT—Design Optimization Tools (V. 5.0) 1999, Vanderplaats R&D, Inc.

Freund, T. J.; Littell, R. C. 2000: *SAS System for Regression*, 3rd Edition. Cary: SAS Institute, pp. 68-77

Hasofer, A.M.; Lind, N. 1974: An exact and invariant rirst-order reliability format. *Journal of Engineering Mechanics* **100**, 111-121

Jaunky, N.; Knight, N. 1999: An assessment of shell theories for buckling of cylindrical panels. *International Journal of Solid Structures* **36**, 3799-3820

Liaw, L. D.; DeVries, R. I. 2001: Reliability-based optimization for robust design. *International Journal of Vehicle Design* **25**, 64-77

Liu, Y. W.; Moses, F. 1994: A sequential response surface method and its application in the reliability analysis of aircraft structural systems. *Structural Safety* **16**, 39-46

Madson, H. O.; Krenk, S.; Lind, N. C. 1986: Methods of Structural Safety. New Jersey: Prentice-Hall, Inc., pp. 120–123

NESSUS (V. 7.0) 2002, Southwest Research Institute.

Polykin, A. A.; van Keulen, F.; Toropov, V. V. 1995: Optimization of geometrically nonlinear thin-walled structures using the multipoint approximation method. *Structural Optimization* **9**, 105-116

Rackwitz, R.; Fiessler, B. 1978: Structural reliability under combined random load sequences. *Computers and Structures* **9**, 489-494

Sevant, N. E.; Bloor, M. I. G.; Wilson, M. J. 2000: Aerodynamic design of a flying wing using response surface methodology. *Journal of Aircraft* **37**, 562-569

Shinozuka, M. 1983: Basic analysis of structural safety. *Journal of the Structural Division*, ASCE, Vol. **109**, 721–740

Stroud, A. H.; Secrest, D. 1963: Approximate integration formulas for certain spherically symmetric regions. *Mathematics of Computation* **17**, 105-135

Torng, T. Y.; Lin, H.-Z.; Khalessi, M. R. 1996: Reliability calculation based on a robust importance sampling method. *Proc. 37th AIAA/ASME/ASCE/ AHS/ASC Structures, Structural Dynamics, and Materials Conference* (held in Salt Lake City, UT) pp. 1316-1325

Toropov, V. V.; Filatov, A. A.; Polykin, A. A. 1993: Multiparameter structural optimization using FEM and multipoint explicit approximations. *Structural Optimization* **6**, 7-14

VisualDOC—Design Optimization Software (V. 3.0) 2002, Vanderplaats R&D, Inc.

Wu, Y-T. 1994: Computational methods for efficient structural reliability and reliability sensitivity analysis. *AIAA Journal* **32**, 1717-1723

Zhou, J-H.; Nowak, A. 1988: Integration formulas to evaluate functions of random variables. *Structural Safety* **5**, 267-284

Appendix A
Shell buckling analysis

The computational model used in buckling analysis of circular cylinders is a semicircular shell with the unloaded edges having symmetric boundary conditions and the loaded edges treated as clamped as shown in Fig. A1. This model falls under the general category of thin-shell structures with the displacement field described by the first-order shear deformation theory formulated as

$$\begin{aligned} u(x,y,z) &= u_0(x,y) + z\phi_x(x,y) \\ v(x,y,z) &= v_0(x,y) + z\phi_y(x,y) \\ w(x,y,z) &= w_0(x,y) \end{aligned} \tag{A1}$$

where u_0, v_0, w_0 are the midplane displacements in x, y, z directions (see Fig. A1), respectively, and ϕ_x, ϕ_y describe rotations about the y and x axes, respectively.

The strain-displacement relations are based on Sanders-Koiter shell theory with the in-plane strains ($\varepsilon_x^0, \varepsilon_y^0, \gamma_{xy}^0$, at $z = 0$), transverse shear strains ($\gamma_{xz}^0, \gamma_{yz}^0$, at $z = 0$), and curvatures ($\kappa_x, \kappa_y, \kappa_{xy}$) formulated as

$$
\begin{aligned}
\varepsilon_x^0 &= \frac{\partial u_0}{\partial x} \\
\varepsilon_y^0 &= \frac{\partial v_0}{\partial y} + \frac{w_0}{R} \\
\gamma_{xy}^0 &= \frac{\partial u_0}{\partial y} + \frac{\partial v_0}{\partial x} \\
\kappa_x &= \frac{\partial \phi_x}{\partial x} \\
\kappa_y &= \frac{\partial \phi_y}{\partial y} \\
\kappa_{xy} &= \frac{\partial \phi_x}{\partial y} + \frac{\partial \phi_y}{\partial x} + \frac{1}{2R}\left(-\frac{\partial u_0}{\partial y} + \frac{\partial v_0}{\partial x}\right) \\
\gamma_{xz}^0 &= \phi_x + \frac{\partial w_0}{\partial x} \\
\gamma_{yz}^0 &= \phi_y + \frac{\partial w_0}{\partial y} - \frac{v_0}{R}
\end{aligned}
\tag{A2}
$$

where R is the shell radius of curvature in y direction (see Fig. A1). Hence, the elastic strain energy stored in the shell can be expressed as

$$
U = \frac{1}{2}\int_A \{\varepsilon\}^T \begin{bmatrix} A_{ij} & B_{ij} & 0 \\ & D_{ij} & 0 \\ \text{sym} & & C_{pq} \end{bmatrix} \{\varepsilon\} dA \tag{A3}
$$

where A_{ij}, B_{ij}, D_{ij} are the laminate extensional, coupling, and bending stiffness matrices, respectively, and C_{pq} is the transverse shear stiffness matrix with the strain vector defined as

$$
\{\varepsilon\}^T = \left\{\varepsilon_x^0 \ \varepsilon_y^0 \ \gamma_{xy}^0 \ \kappa_x \ \kappa_y \ \kappa_{xy} \ \gamma_{xz}^0 \ \gamma_{yz}^0\right\}^T \tag{A4}
$$

The work done by the applied edge load (see Fig. A1) is calculated using the nonlinear components of strain-displacement relations with the resulting equation expressed as

$$
W = \frac{1}{2}\int_A \overline{N}_x \left[\left(\frac{\partial v_0}{\partial x}\right)^2 + \left(\frac{\partial w_0}{\partial x}\right)^2\right] dA \tag{A5}
$$

where $\overline{N}_x$ is the stress resultant in the x direction.

To obtain the critical buckling load, the displacements u_0, v_0, w_0 and rotations ϕ_x, ϕ_y are approximated by different Ritz series with Legendre polynomials used as the interpolation functions such that the essential boundary conditions are satisfied. Then through the application of the principle of minimum total potential energy the critical buckling load is found by setting Eqs. (A3) and (A5) equal to each other and solving the resulting eigenvalue problem for the critical load factor such that

$$N_{cr} = \lambda_{cr} N_x \tag{A6}$$

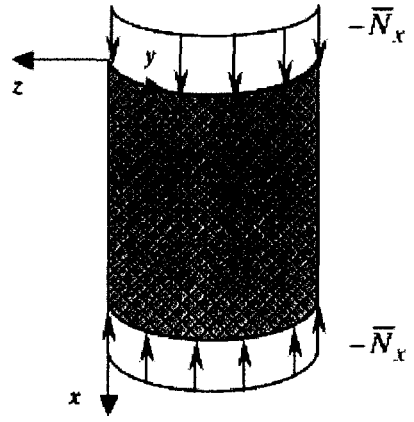

Fig. A1 Computational model of circular cylinder

A computer implementation of the described analysis procedure developed by Jaunky and Knight (1999) is used to generate the necessary response samples for development of GRS and LRS models.

Prior to its use, we compared the results obtained from this code with those from linear buckling analysis in MSC/NASTRAN. The latter solutions were based on a 60 x 216 finite element model of the complete cylinder with approximately 76,700 total degrees of freedom. The critical buckling loads obtained from these two programs were found to be in excellent agreement.

Appendix B
Selection of design points based on quadrature formulae

The approach we refer to as Quadrature design for fitting a linear RS model is based on targeted sampling of design space at n+1 points corresponding to n+1 vertices of a regular n-simplex with centroid at the origin. The coordinates of ith design point are obtained using the relationship

$$x_{i,j} = \mu_{X_j} + Z_{i,j}\sigma_{X_j} \qquad \begin{matrix} i = 1,2,...,n+1 \\ j = 1,2,...,n \end{matrix} \tag{B1}$$

where μ_{X_j}, σ_{X_j} represent the mean value and standard deviation of jth random variable, respectively, and $Z_{i,j}$ is the perturbation vector at ith design point.

The elements of $z_{i,j}$ correspond to the quadrature points developed by Stroud and Secrest (1963) for approximate solution of multiple integrals of polynomial functions involving two or more independent variables, and later used by Zhou and Nowak (1998) for non-product point integration of a function of multiple normal random variables.

At the first design point, the perturbation vector is given as

$$Z_{1,j} = (z_{1,1}, z_{1,2}, ..., z_{1,n}) = (\sqrt{n}, 0, 0, ..., 0) \tag{B2}$$

Therefore, while the first design variable is perturbed from its mean value by $\sqrt{n}\sigma_{X_1}$, the remaining variables are kept at their respective mean values. For the subsequent n design points (see Fig. B1), the perturbation vector is defined as

$$Z_{2,j} = \left(-\sqrt{\frac{1}{n}}, \sqrt{\frac{(n+1)(n-1)}{n}}, 0, ..., 0\right)$$

$$Z_{3,j} = \left(-\sqrt{\frac{1}{n}}, -\sqrt{\frac{(n+1)}{n(n-1)}}, \sqrt{\frac{(n+1)(n-2)}{(n-1)}}, 0, ..., 0\right)$$

. . . . (B3)

$$Z_{n,j} = \left(-\sqrt{\frac{1}{n}}, -\sqrt{\frac{(n+1)}{n(n-1)}}, -\sqrt{\frac{(n+1)}{(n-1)(n-2)}}, -\sqrt{\frac{(n+1)}{(n-2)(n-3)}}, ..., \sqrt{\frac{(n+1)}{2}}\right)$$

$$Z_{n+1,j} = \left(-\sqrt{\frac{1}{n}}, -\sqrt{\frac{(n+1)}{n(n-1)}}, -\sqrt{\frac{(n+1)}{(n-1)(n-2)}}, -\sqrt{\frac{(n+1)}{(n-2)(n-3)}}, ..., -\sqrt{\frac{(n+1)}{2}}\right)$$

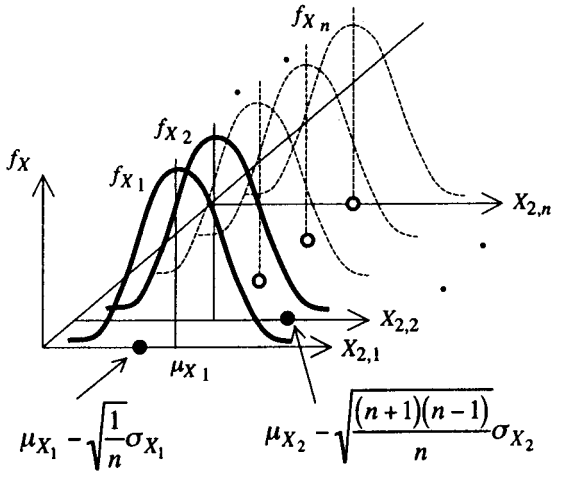

Fig. B1 Depiction of random values selected for design point 2